Extension of the high-ion-temperature regime in the Large Helical Device[a)]

M. Yokoyama,[b)] K. Nagaoka, M. Yoshinuma, Y. Takeiri, K. Ida, S. Morita, O. Kaneko, T. Seki, H. Kasahara, T. Mutoh, Y. Oka, K. Tsumori, M. Osakabe, K. Ikeda, K. Tanaka, H. Funaba, S. Matsuoka, S. Masuzaki, J. Miyazawa, R. Sakamoto, H. Yamada, K. Kawahata, N. Ohyabu, S. Imagawa, A. Komori, S. Sudo, O. Motojima, and the LHD Experimental Group
National Institute for Fusion Science, 322-6 Oroshi, Toki 509-5292, Japan

(Received 16 November 2007; accepted 13 February 2008; published online 25 March 2008)

High-ion-temperature (exceeding 5 keV) hydrogen plasmas have been successfully produced in the Large Helical Device [Iiyoshi *et al.*, Nucl. Fusion **39**, 1245 (1999); Motojima *et al.*, Nucl. Fusion **47**, S668 (2007)] with the ion heat confinement improvement in the core region. The experimental ion heat diffusivity at the core region is found to be almost independent of the ion temperature, T_i (even decreasing as T_i increases). The neoclassical (NC) ripple transport is suppressed by the ambipolar radial electric field, E_r (<0) predicted by NC transport fluxes. The temperature ratio, T_i/T_e, is one of the key parameters to reduce the NC ambipolar particle and heat fluxes. Thus, it is suggested that the selective ion heating (making T_i/T_e larger) is a plausible approach to further increase T_i. Spontaneous rotation is evaluated in these high-T_i plasmas, in which a co-directed component is recognized at the radial location with a large T_i gradient, in addition to the tokamak-like counter-directed component expected for $E_r<0$. © *2008 American Institute of Physics*. [DOI: 10.1063/1.2890755]

I. INTRODUCTION

The Large Helical Device (LHD)[1] is the world's largest superconducting helical device, which has significantly extended the high-performance regime of magnetic confinement research in helical systems, and also has demonstrated long-pulse capability, which is an inherent advantage provided by the helical magnetic configuration.[2] The capability of high-ion-temperature plasma confinement is also one of the key issues to be demonstrated.

It has been known that the temperature ratio (T_i/T_e) is one of the important parameters to determine the plasma confinement properties. Here, T_e and T_i denote the electron and ion temperatures, respectively. For example, particle and heat transport improve as T_i/T_e is increased, as recognized in DIII-D.[3] The damping rate of the zonal flow is predicted to depend on the radial electric field (E_r) in helical plasmas, where E_r is strongly affected by the temperature ratio,[4] through the ambipolarity condition based on neoclassical (NC) particle fluxes.[5]

LHD plasmas typically have had a higher T_e than T_i due to the electron-predominant heating from the high-energy neutral beam injection (NBI) heating. The NC ambipolar E_r in such $T_e/T_i>1$ plasmas tends to be positive (electron root), and the impact of the positive E_r on confinement properties and improvement have been extensively studied in LHD[6–8] and also in other helical devices.[9]

On the other hand, helical plasmas with $T_i>T_e$ are predicted to have a negative ambipolar E_r as systematically evaluated in Ref. 5. In this regard, the ion heating experiments in LHD are significant not only to demonstrate the high-T_i plasma confinement capability, but also to extend the plasma parameter regime to $T_i>T_e$ so that the impact of the negative E_r on helical plasma confinement can be widely studied, and also to comprehensively understand the impact of temperature ratio on helical plasmas.

To demonstrate high-T_i plasma confinement capability in LHD, high-Z (such as Ne and Ar) plasmas with low ion density (in the range of 10^{18} m^{-3}) were used as targets during the period when only tangential NBIs were operating, to effectively increase the absorption power per ion. T_i of about 13.5 keV was successfully demonstrated by this approach.[10] More importantly, it was found that the scaling between the achieved T_i and the absorbed power normalized by the ion density is almost similar regardless of the ion species. This successful proof-of-principle ion heating experiment has encouraged the installation and power increase (up to 6–7 MW) of a low-energy (40 keV) perpendicular NBI to increase the direct ion-heating power. As a result, T_i has now exceeded 5 keV in a hydrogen plasma, which extends the high-T_i regime in helical system research. The core of the high-T_i plasma is characterized by $T_i/T_e>1$, which provides a new parameter regime for LHD plasmas. It should also be mentioned that this low-energy NBI is perpendicularly injected, enabling the charge exchange spectroscopy (CXS) measurement with a toroidal line of sight for measuring radial profiles of T_i and toroidal rotation (V_t) even in cases with a hollow impurity density profile (carbon is utilized for the measurement).[11] The observation of T_i and V_t profiles has enhanced the physics understandings of ion confinement in helical plasmas.

This paper is organized as follows. In Sec. II, heating equipment for ion heating experiments in LHD is explained. Plasmas with $T_i>5$ keV are described in Sec. III including the ion heat confinement properties in such plasmas. The

[a)] Paper GI2 1, Bull. Am. Phys. Soc. **52**, 98 (2007).
[b)] Invited speaker. Author to whom correspondence should be addressed. Electronic mail: yokoyama@LHD.nifs.ac.jp.

utilization of ambipolar E_r for higher-T_i plasma production (toward the reactor relevant regime) is also suggested based on the current understanding of the obtained high-T_i plasmas in LHD. Spontaneous rotation is also briefly mentioned. Finally, a summary and discussion will be given in Sec. IV.

II. SETUP FOR ION HEATING EXPERIMENTS IN LHD

The LHD is equipped with three tangential negative-ion-based and one recently installed perpendicular positive-ion-based NBI, in which the nominal injection energy of the hydrogen beam is as high as 180 keV (for the tangential beams)[12] and 40 keV (for the perpendicular beam). The tangential NBIs were designed to achieve a high fusion triple product and the injection energy was determined for target densities of $(3-5)\times10^{19}$ m^{-3}. For lower-density hydrogen plasmas, however, most of the beam power goes to electrons due to the high injection energy. The total injection power of the three tangential NBIs has reached about 14 MW. One injector (No. 2) has the opposite injection direction to the other two injectors (Nos. 1 and 3). A low-energy NBI (No. 4) began operation in 2005, and 7 MW injection was achieved in the last experimental campaign (2006–2007).

Ion cyclotron range of frequency heating (ICH)[13] can also be utilized since the target plasmas for ion heating experiments in LHD recently has been the low-Z species, like hydrogen and/or helium. A total power of about 2 MW (38.47 MHz) was injected through four antennas with the minority heating mode. The resonance layer of the minority heating mode is located near the core region for a case with R_{ax}=3.60 m and B=2.75 T. Here, R_{ax} denotes the magnetic axis position and $B$is the magnetic field strength.

The electron cyclotron range of frequency heating (ECH) has also been recognized to be effective to improve ion confinement at the core region through the appearance of the electron root E_r with a large positive value. This effect was clearly recognized at the electron density of about 0.3×10^{19} m^{-3} in high-Z plasmas.[14] The target density for ion heating experiments described in this paper is above 1×10^{19} m^{-3}. In such a density regime, clear effects of ECH on ion confinement have not yet been observed, although the increase of the T_i gradient (T_i is in the range of 1 keV) at the core region associated with a co-toroidal rotation enhancement was observed.[15]

III. HIGH-ION-TEMPERATURE HYDROGEN PLASMAS IN LHD

A. High-T_i hydrogen plasma production in LHD

High-T_i hydrogen plasmas with $T_i>5$ keV were successfully produced. Figure 1 shows the results of a 5.2 keV discharge at a density of about 1.2×10^{19} m^{-3}, where the following results are shown: (a) T_i (CXS), (b) T_e (Thomson scattering), (c) V_t (CXS) profiles, and (d) the heating scenario. The magnetic configuration is characterized by R_{ax}=3.575 m with B=−2.769 T (reversed magnetic field direction), which makes two tangential beams (Nos. 1 and 3) co-injection and No. 2 counter-injection. The low-energy beam (No. 4) consists of four ion sources with the two independently operatable power supply systems (4A and 4B). This flexibility is utilized to modulate one of power supplies (in this case, 4B) to modulate the injection with 100 ms interval to obtain the background signals of CXS measurement, as seen at the bottom of Fig. 1(d).

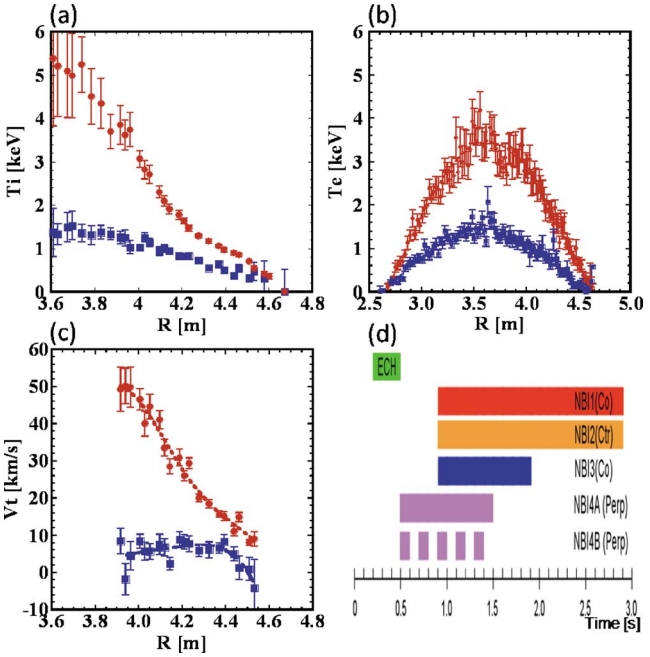

FIG. 1. (Color online) (a) T_i, (b) T_e, (c) V_t profiles at t=0.75 s (■) and t=1.15 s (●), and (d) the heating scenario for a 5.2 keV-T_i discharge.

The No. 4 beam was injected for 1 s from t=0.5 s (just after the ECH turn-off), with the superposition of Nos. 1–3 beams from t=0.9 s. At the timing of No. 4 only (t=0.75 s), T_i reaches about 1.6 keV with comparable T_e. The density profile at this timing is peaked with the particle fueling from No. 4 beam.[16] The V_t is rather small (less than 10 km/s) at t=0.75 s. Once the Nos. 1–3 beams are injected in addition to the beam No. 4, T_i increases and reaches 5.2 keV at the core region with the apparent change of the gradient around $R\sim4.2$ m. In this high-T_i phase, T_i exceeds T_e [~3.5 keV at the core region as seen in Fig. 1(b)]. The density profile tends to become flat to hollow at this timing, which is a typical trend for tangential beam injection in LHD. The V_t is also largely enhanced in the co-direction in accordance with the predominance of co-injected beams. The V_t at the very core region is difficult to measure due to the lack of the line intensity for the measurement. However, at least as much as 50 km/s of V_t (about 7% of the thermal velocity of the hydrogen ion with 5.2 keV) is observed.

There is another example of a high-T_i discharge with ICH at a higher density of about 1.6×10^{19} m^{-3}, as shown in Fig. 2: (a) T_i and (b) V_t profiles, and (c) the heating scenario. In this case, the ICH (~2 MW) is superimposed on the No. 4 beam just after ECH turn-off and followed by the further superposition of the Nos. 1–3 beams from 1.1 s. The magnetic configuration is R_{ax}=3.6 m with B=2.85 T (normal direction), making counter-injection dominant (Nos. 1 and 3 are counter-injection). The T_i reaches above 2 keV (at the density range of about 1.6×10^{19} m^{-3}) during the phase of

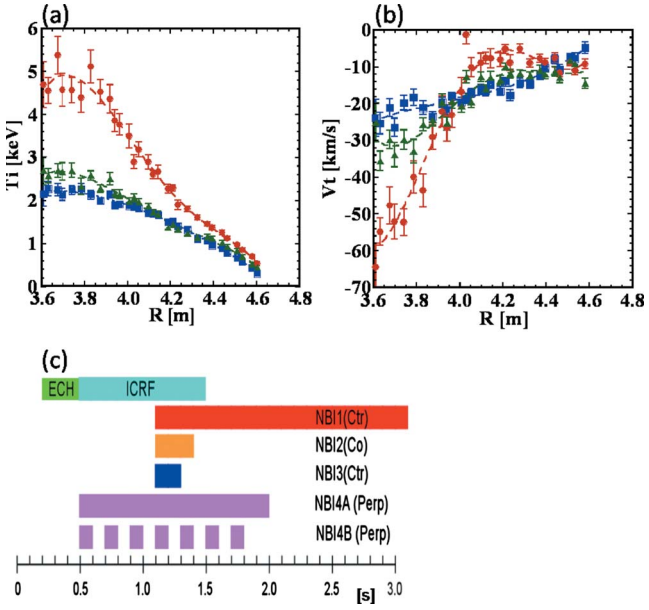

FIG. 2. (Color online) (a) T_i and (b) V_t profiles at $t=0.95$ s (■), $t=1.35$ s (●), and $t=1.75$ s (▲), and (c) the heating scenario for a 5 keV-T_i discharge with ICH.

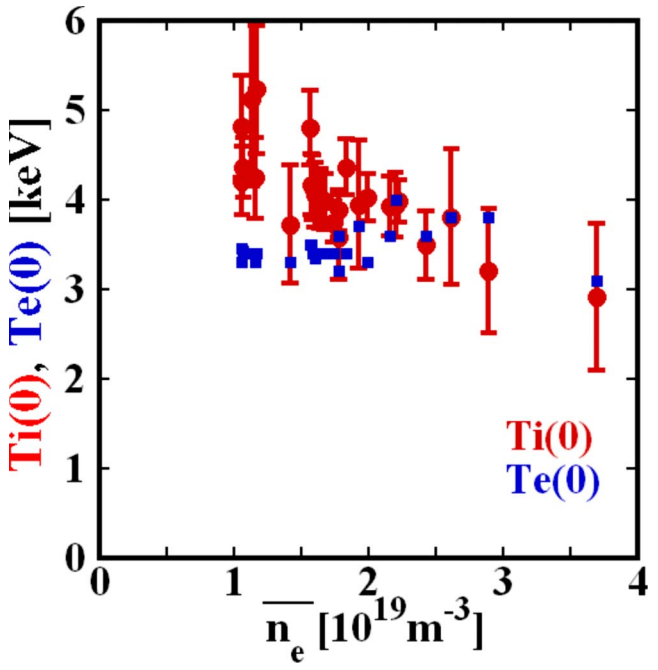

FIG. 3. (Color online) Core T_i (●) and T_e (■) as a function of the electron density for a density scan experiment.

No. 4 beam injection and ICRH and further increases up to about 5 keV 200–300 ms after the Nos. 1–3 beam injections. The V_t is also enhanced in the counter-direction at the timing of the maximum T_i. It is also noted that the core T_e changes from about 2 to 3.5 and then 3 keV at $t=0.95$, 1.35, and 1.75 s, respectively. Thus, $T_i > T_e$ is again the case at the timing of the maximum T_i.

The density scan experiments were also performed as summarized in Fig. 3, where the core T_i and T_e are plotted as a function of the electron density deduced from the FIR measurement. It is clearly recognized that $T_i > T_e$ at the lower density regime and then T_i tends to become comparable to T_e (due to the energy equipartition) as the density is increased. T_i reaches 3 keV even at $n_e > 3 \times 10^{19}$ m^{-3}.

B. Ion heat confinement properties

The ion heat confinement properties of high-T_i plasmas are described to clarify the confinement characteristics of these high-T_i plasmas.

First, ion thermal diffusivity (χ_i) is described from the viewpoint of both the experimental and NC one. For the experimental ion thermal diffusivity ($\chi_{i,\mathrm{exp}}$) analysis, an NBI deposition calculation is performed using the FIT code, which can analyze the NBI heating profiles in a 3D magnetic configuration assuming a quasi-steady-state plasma. It is a reduced-version of the GNET code.[17,18] The GNET code can evaluate the accurate deposition profile and distribution in the velocity space of injected beam particles based on the Monte Carlo approach in 5D phase space. For the purpose of the application of this time-consuming GNET code to the experimental analysis, it has been reduced to the FIT code by considering that the full-orbit effect during the slowing-down process on the deposition profile evaluation is not necessary, and that the prompt orbit loss effect is a sufficient approximation for such a purpose.

Here, the effective Z of the background plasma is assumed to be 2. It has been confirmed that changing Z from 2 to 3 gives only a slight change in the deposited power and therefore the estimation of $\chi_{i,\mathrm{exp}}$.

Figure 4(a) shows $\chi_{i,\mathrm{exp}}$ (normalized by a Gyro-Bohm factor, $T_i^{1.5}$) at a radial location from near the center to $\rho \sim 0.6$ for the lower- and higher-T_i cases shown in Fig. 1(a). The reduction of $\chi_{i,\mathrm{exp}}$ is recognized, especially about a two orders of magnitude (in $\chi_{i,\mathrm{exp}}/T_i^{1.5}$) reduction occurs at the core region. This clearly indicates that the ion heat confinement is largely improved at the core of a higher-T_i plasma.

A change of the T_i gradient ("foot-point") can be observed at $R \sim 4.2$ m (corresponding to $\rho \sim 0.7$). Since a global T_i fitting (from $\rho=0$ to $\rho=1$) may miss this local structure, a closer look at the T_i gradient is performed in the radial location of $R \sim 4$–4.4 m, as shown in Fig. 4(b). It is clearly seen that there is a discontinuity in the T_i gradient, indicating that the ion heat confinement property is qualitatively different between the outer and inner region separated by a foot-point. It can be even quantitatively shown by evaluating the $\chi_{i,\mathrm{exp}}$ utilizing the locally evaluated T_i gradient. Such an estimate is shown in Fig. 4(c), where the spatial jump and the change of the slope of $\chi_{i,\mathrm{exp}}$ are recognized for the higher-T_i case. Based on these facts, it can be concluded that a high-T_i plasma is obtained as a result of the improved confinement mode, not just a result of the gradual increase of T_i.

It is also important to investigate the contribution from the NC transport in helical plasmas especially in the low-collisionality regime since the enhancement of heat and particle diffusion is anticipated due to the predicted ripple transport with an unfavorable dependence on $1/\nu$, where ν is the collision frequency. The NC transport analysis has been per-

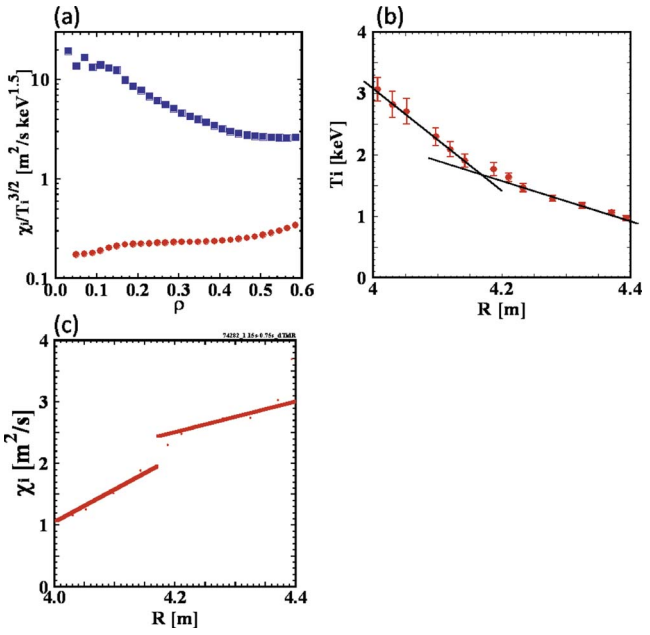

FIG. 4. (Color online) (a) $\chi_{i,\mathrm{exp}}$ (normalized by $T_i^{1.5}$) at the radial locations from $\rho \sim 0.6$ to the center of the lower- (■) and higher- (●) T_i cases shown in Fig. 1(a). (b) A closer look ($4 < R < 4.4$ m) at the T_i gradient and (c) $\chi_{i,\mathrm{exp}}$ estimated utilizing the locally evaluated T_i gradient [Fig. 4(b)] for a higher-T_i case.

formed for the case shown in Fig. 1 by using the GSRAKE code.[19] The NC diffusion coefficients are evaluated by utilizing the experimentally obtained density and temperature profiles to obtain the electron and ion particle fluxes (Γ_e and Γ_i). The ambipolar condition, $\Gamma_e = \Gamma_i$, provides the ambipolar E_r. Unfortunately, due to the hollow carbon impurity profiles, E_r has not yet been measured at the core region of such high-T_i plasmas. Thus, the NC ambipolar E_r is the only available information on E_r. However, it is fair to think that the NC ambipolar E_r gives a rather good indication for the experimentally observed E_r in LHD as demonstrated in previous papers.[9,20]

The estimated ambipolar E_r at $t=0.75$ s [$T_i(0) \sim 1.6$ keV] and 1.15 s (~ 5.2 keV) are shown in Fig. 5(a). A negative E_r is anticipated all the way from the core to the edge for both cases, with a slight enhancement in the core region for the higher-T_i case. The positive E_r is also predicted in an isolated narrow peripheral region for the higher-T_i case, which is not shown in Fig. 5(b) [so as in Fig. 9(b)]. Figure 5(b) shows the NC ion heat diffusivity ($\chi_{i,\mathrm{NC}}$) with the ambipolar E_r (<0) taken into account. The $\chi_{i,\mathrm{NC}}$ shows little change in the core region between the two cases even with an almost tripled T_i in the higher-T_i case compared to that of the lower-T_i case. It should be also noted that $\chi_{i,\mathrm{NC}}$ is predicted to be about three orders of magnitude larger (up to $\sim 10^3$ m^2/s) in the higher-T_i case if E_r is assumed to be zero ("pure" ripple transport). The ambipolar E_r plays a significant role in preventing the theoretically predicted ripple transport level to appear. Figure 6 shows NC ion and electron fluxes as a function of E_r at $\rho=0.2$ for the (a) lower- and (b) higher-T_i cases. A significantly larger Γ_i is predicted to appear at $E_r=0$ in the higher-T_i case compared to that in the lower-T_i case. However, the NC ambipolarity assures a negative E_r so that the realizable level of the NC particle flux remains comparable to that obtained in (a). In this regard, it can be said that the ripple transport can be well suppressed by the presence of ambipolar E_r even in this high-T_i plasma.

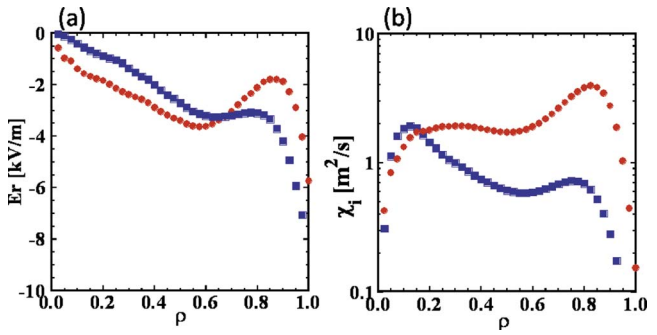

FIG. 5. (Color online) (a) E_r evaluated from NC ambipolarity, and (b) $\chi_{i,\mathrm{NC}}$ (ambipolar E_r taken into account) for lower- (■) and higher- (●) T_i cases shown in Fig. 1(a).

A comparison between $\chi_{i,\mathrm{exp}}$ and $\chi_{i,\mathrm{NC}}$ is shown as a function of T_i (at the core region with $\rho=0.4$) taking the obtained high-T_i discharges as examples, which is shown in Fig. 7(a). Additional cases of comparison should be made, but the trend can be already seen from this figure. The experimental χ_i is greater than the NC one (by about an order of magnitude) in the lower-T_i case. The experimental χ_i remains almost unchanged (even decreasing a bit) as T_i increases, indicating that high-T_i plasmas do not follow a Gyro-Bohm scaling ($\sim T^{1.5}$), thus showing an improvement of the ion heat confinement. The $\chi_{i,\mathrm{NC}}$ is increasing as $T_i^{1.17}$, whose power law is much smaller than the $T_i^{4.5}$ predicted theoretically in a "pure" ripple transport. The $\chi_{i,\mathrm{exp}}$ and $\chi_{i,\mathrm{NC}}$ become comparable at $T_i \sim 4$ keV in these examples. However, $\chi_{i,\mathrm{NC}}$ can be further reduced by enhancing the ion-root E_r, for example, by increasing the T_i/T_e ratio. Figure 7(b) shows Γ_e and Γ_i at $\rho=0.2$ for the higher-T_i case shown in Fig. 1(a). It clearly shows that Γ_i is reduced to the level of Γ_e. The T_i/T_e is about 1.4 in this case, where the ripple transport enhancement (at $E_r=0$) of Γ_e begins to appear. If T_e is lowered artificially to make the ratio $T_i/T_e=4$, such an enhancement does not appear, and Γ_e is further decreased to

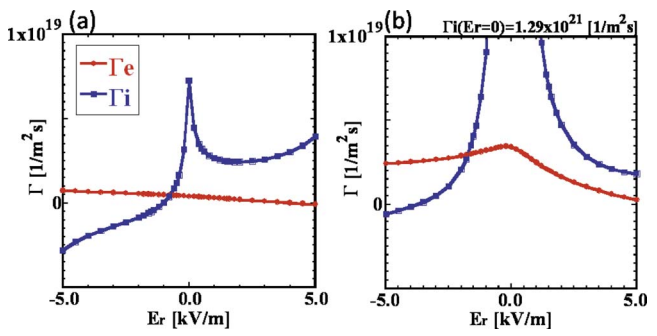

FIG. 6. (Color online) NC ion (■) and electron (●) fluxes as a function of E_r at $\rho=0.2$ for the (a) lower- and (b) higher-T_i cases shown in Fig. 1(a).

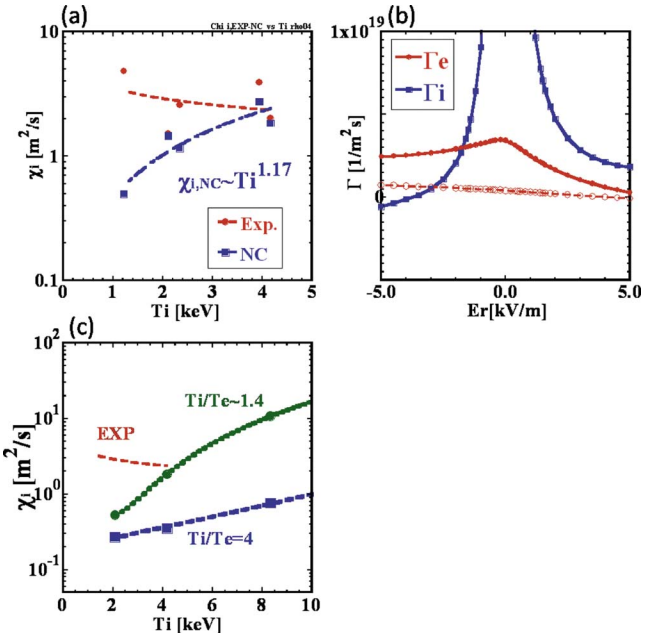

FIG. 7. (Color online) (a) Comparison between $\chi_{i,\mathrm{exp}}$ (● and chain curve for fitting) and $\chi_{i,\mathrm{NC}}$ (■ and chain-dotted curve for fitting) is shown as a function of T_i (at the core region with $\rho=0.4$). (b) Γ_e and Γ_i at $\rho=0.2$ of the higher-T_i case shown in Fig. 1(a). The case with the artificially reduced T_e (to make T_i/T_e larger) is also shown (○). (c) $\chi_{i,\mathrm{NC}}$ evaluated by T_i-scan calculations for $T_i/T_e=1.4$ and 4 as a function of T_i (up to 10 keV), by taking the parameters at $\rho=0.4$ of a higher-T_i case shown in Fig. 1(a) as the baseline. For reference, the fitting curve of $\chi_{i,\mathrm{exp}}$ shown in Fig. 7(a) is also plotted.

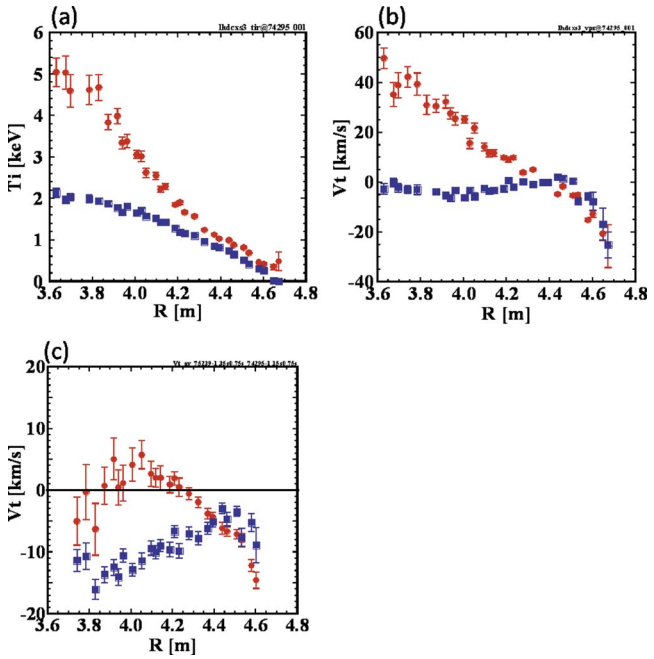

FIG. 8. (Color online) (a) T_i and (b) V_t profiles for lower- (■) and higher- (●) T_i cases for a co-dominant NBI heated plasma. (c) V_t profiles for lower- (■) and higher- (●) T_i cases, obtained by averaging the V_t profiles of Figs. 2(b) and 8(b).

decrease the ambipolar flux as well. This reduction is more systematically seen in Fig. 7(c), where the calculations are performed by taking the parameters at $\rho=0.4$ of a higher-T_i case shown in Fig. 1(a) as the baseline, and $\chi_{i,\mathrm{NC}}$ is evaluated for cases with $T_i/T_e=1.4$ and 4, by varying T_i while fixing the density to be the same as that of the case shown in Fig. 1(a) ($\sim 1.2\times 10^{19}$ m^{-3}). The equilibrium of the case in Fig. 1(a) is employed throughout the parameter scan calculations. Therefore, results for more than ~4 keV are underestimated. Nevertheless, $\chi_{i,\mathrm{NC}}$ is much reduced in the case with $T_i/T_e=4$, which suggests that the selective ion heating (making T_i/T_e higher) should be an effective approach for the further increase of T_i.

However, in the higher density regimes such as those relevant to a reactor, decoupling the ions and electrons is unrealistic. In such a case, i.e., for the case of comparable T_e/T_i, Γ_e enhancement due to the appearance of the electron's ripple transport can be utilized to make the electron root possible. Such an estimate has been carried out in Ref. 21, where it is reported that the electron-root scenario for the reactor-relevant density regime with $T_e\sim T_i$ in the range of 10 keV is possible with more than one order of magnitude reduction of $\chi_{i,\mathrm{NC}}$ compared to that for the ion-root case.

C. Spontaneous rotation

Transport in the plasma is considered to be sensitive to the profile of the flow velocity. The mechanism for driving the spontaneous toroidal flow is of great interest in the area of momentum transport physics and has been investigated experimentally and theoretically.[22–27] Besides the toroidal flow driven by the external momentum input of the tangential NBI, there is the spontaneous toroidal flow driven by the coupling of the $\boldsymbol{E}\times\boldsymbol{B}$ force and the viscosity tensor. The stress tensor redirects some fraction of the diamagnetic and $\boldsymbol{E}\times\boldsymbol{B}$ flows into parallel flows.

In the following, the observed toroidal flow is described together with an estimate of the spontaneous rotation in high-T_i plasmas in LHD.

High-T_i plasmas have been obtained in LHD in configurations either in the normal or in the reversed magnetic field direction, as shown in Figs. 1 and 2. As described there, toroidal rotation is enhanced in the direction of the dominant tangential NBI. Here, two almost identical (from the viewpoint of T_i values and profiles, plasma density and injection power, etc.) high-T_i discharges are considered. One is the discharge shown in Fig. 2 (counter-dominant NBI) and the other is shown in Fig. 8 [(a) T_i and (b) V_t profiles] for co-dominant NBI. To estimate the spontaneous rotation contribution on these measured V_t, the average of these two discharges is performed (both in higher- and lower-T_i cases) so that the toroidal flow driven by the external momentum input from tangential NBIs can be canceled out. Such an averaging has resulted in profiles as shown in Fig. 8(c). For the lower-T_i case, the spontaneous toroidal flow is in the counter-direction. It is noted that the predicted E_r is negative in these cases [as shown in Fig. 5(a)]. The core region of the LHD magnetic configuration is dominantly governed by toroidicity rather than helicity due to their ρ dependences such as $\sim\rho$ and $\sim\rho^2$, respectively, from which it can be very roughly considered that the magnetic configuration of the core region of LHD is similar to that of tokamaks. Spontaneous rotation in tokamaks in the case of negative E_r is directed in the

counter-direction.[25] Thus, the counter-rotation estimated in the lower-T_i cases shown in Fig. 8(c) can be understood as a property similar to that in tokamaks. On the other hand, for higher-T_i cases, the contribution toward the co-direction is recognized by considering the difference between higher- and lower-T_i cases in Fig. 8(c). This contribution is pronounced at the radial region where the T_i gradient becomes large [cf. Figs. 2(a) and 8(a)]. Since the E_r is predicted to be negative also in these high-T_i cases, this co-direction contribution should be based on a mechanism other than E_r, and it might be related to the T_i gradient (then pressure gradient). The mechanism for this observation has not yet been understood, and remains an open issue.

IV. SUMMARY AND DISCUSSIONS

High-ion-temperature (exceeding 5 keV) hydrogen plasmas have been successfully produced in LHD. Such high-T_i plasmas are obtained by the improvement of ion heat confinement associated with a change of the T_i gradient. It is also revealed that the neoclassical ripple transport is well suppressed by the ambipolar $E_r(<0)$. It is found, from the comparison between experimental and NC ion heat diffusivity, that the NC level is approaching the experimental one as T_i increases in analyzed high-T_i plasmas. The temperature ratio, T_i/T_e, is one of the key parameters to reduce the NC ambipolar particle and heat fluxes. It is suggested that selective ion heating (making T_i/T_e larger) is a plausible approach to further increase T_i by making the ion root E_r larger (in absolute value) with the current LHD heating equipment (ion-root scenario). Of course, for a reactor relevant situation with $T_i \sim T_e$, this approach does not work. For such a case, the electron-root scenario (by utilizing the appearance of the electron's ripple transport) is demonstrated.[21]

Spontaneous rotation is also evaluated in these high-T_i plasmas, in which the co-directed component is recognized at the radial location with a large T_i gradient, in addition to the tokamak-like counter-directed component expected for $E_r<0$. Systematic analyses for spontaneous rotation in high-T_i plasmas are ongoing tasks.

The NC analyses beyond the radial transport, such as plasma flows and their relationships with parallel/perpendicular viscosities, have been initiated as described in the Appendix. Such analyses will increase the understanding of plasma flow issues in helical plasmas and their impacts on confinement properties along with experimental verifications in LHD.

Finally, the evaluation of the ambipolar E_r is discussed. Previously in Wendelstein 7-A, it was demonstrated that the ion energy confinement was strongly improved by building up large negative E_r through enhancing the fast ion loss by the perpendicular NBI.[28,29] In this paper, the contribution from fast ion loss in the determination of the ambipolar E_r was neglected. The characteristics supporting this assumption are the following. In LHD, ions are found to be heated up to the MeV range by ICH,[30] which indicates that the fast ions are well confined without experiencing direct losses. The employed inward-shifted magnetic configurations for these experiments have been evaluated to provide enough power deposition (more than 70% of the injected power can be deposited) from perpendicular NBI. Another characteristic can be found in the electron channel. In LHD (as well as in other helical devices), the energy confinement of core electrons is significantly improved by the appearance of a large positive E_r (electron root) in the core region as is systematically summarized in Ref. 31. In such discharges in LHD, the ambipolar E_r predicted only from neoclassical fluxes (driven by thermal ions and electrons) agrees rather well with the experimentally measured E_r.[32] This finding (although for the electron channel) also supports the estimate of the ambipolar E_r only from the thermal fluxes in this paper. However, even with these supporting features, it is important to check the validity of this assumption by measuring E_r in high-T_i plasmas. The efforts for increasing the measurement capability have been made, such as bundling fiber arrays of the CXS system to increase the background signals even for hollow impurity profiles. It will provide a chance to measure and compare E_r with the estimated ambipolar E_r.

ACKNOWLEDGMENTS

The authors greatly acknowledge all the technical staff for excellent and reliable operation of LHD. Dr. S. P. Hirshman (Oak Ridge National Laboratory) is highly appreciated for his kindness in providing the recent version of the DKES code. Dr. O. Yamagishi and Professor H. Sugama (National Institute for Fusion Science) are also appreciated for their efforts in modifying and testing the DKES code for the application to LHD experimental results.

This work is supported by a Grant-in-Aid (No. 18760638) from the Japanese Ministry of Education, Culture, Sports, Science, and Technology for M.Y., and is also performed with support under the auspices of the NIFS Collaborative Research Program (No. NIFS07KLDD011).

APPENDIX: APPLICATION OF DKES CODE FOR HIGH-T_i PLASMAS IN LHD

The Drift Kinetic Equation Solver (DKES)[33] can solve the linearized DKE and provide mono-energy NC transport coefficients in 3D magnetic configurations, without approximations such as connecting formulas in different collisionality regimes. The mono-energetic transport coefficients can be evaluated at given ν/v and , where ν is the energy-dependent collision frequency and v is the thermal velocity. Since the evaluation of the ambipolar E_r is a key element of the analysis, the module interpolating the mono-energetic transport coefficients on parameters ν/v and E_r/v has been added to the DKES code, so that the ambipolar E_r can be determined by balancing the electron and ion particle fluxes.

The DKES code, with the method of Sugama–Nishimura[34] included, has been applied to analyze high-T_i plasmas in LHD. Calculations for lower- and higher-T_i cases shown in Fig. 1 have been performed, and the evaluated ambipolar E_r is compared with those by GSRAKE [cf. Fig. 5(a)], as shown in Fig. 9. The parameters used

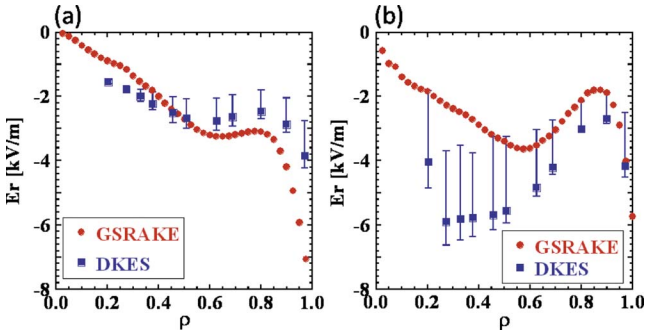

FIG. 9. (Color online) Ambipolar E_r evaluated by DKES (■) and GSRAKE (●) for lower- and higher-T_i cases shown in Fig. 1(a).

for DKES calculations are as follows: (mpol,ntor,mpolb, ntorb,lalpha)=(16,12,6,2,100), where the notations indicate the poloidal and toroidal mode numbers for perturbed distribution functions and the magnetic field expression and Legendre polynomials, in that order. For a case of lower-T_i, DKES and GSRAKE results are fairly close to each other, indicating that particle fluxes themselves are also in good agreement. The convergence of DKES calculations with the min-max variational principle employed is rather well satisfied. On the other hand, for a higher-T_i case, the difference between the two codes becomes apparent especially toward the core region with higher T_i. It is also noted that the range of min-max variation shown by the "error bars" becomes larger there, indicating that the convergence becomes rather poor at lower collisionality.

To examine the convergence properties, the above-mentioned parameters for DKES calculations are varied for the calculation at $\rho \sim 0.37$ of a higher-T_i case shown in Fig. 1(a). Figure 10 shows the parameter dependence of the evaluated ambipolar E_r for several conditions with varied parameters written in the figure. It is noted that "condition 1" corresponds to the result shown in Fig. 9. It seems that the min-max averaged values (circles) tend to become gradually less negative with the increase of mode numbers for the perturbed distribution function (condition 3 to 4) with reduction of the min-max variation. The increase of mode numbers for the magnetic field seems to increase the min-max variation (condition 1 to 2 and 3) with fixed mode numbers for the perturbed distribution function, which indicates that the further increase of mode numbers of the perturbed distribution function is required for larger mode numbers for the magnetic field.

The difference in the evaluated ambipolar E_r between DKES and GSRAKE is still large even for the largest parameters used for DKES calculations (condition 6). Detailed comparison between results from both codes and additional information provided by other NC transport codes (such as DCOM[35]) will be performed soon. It would be necessary to further increase the mode numbers used for DKES calculations when we consider the application to low collisional plasmas like high-T_i plasmas in LHD. It already has been confirmed that DKES and GSRAKE predict almost similar values of ambipolar E_r in collisional plasmas like IDB/SDC (Internal Diffusion Barrier/Super Dense Core) in LHD.[36]

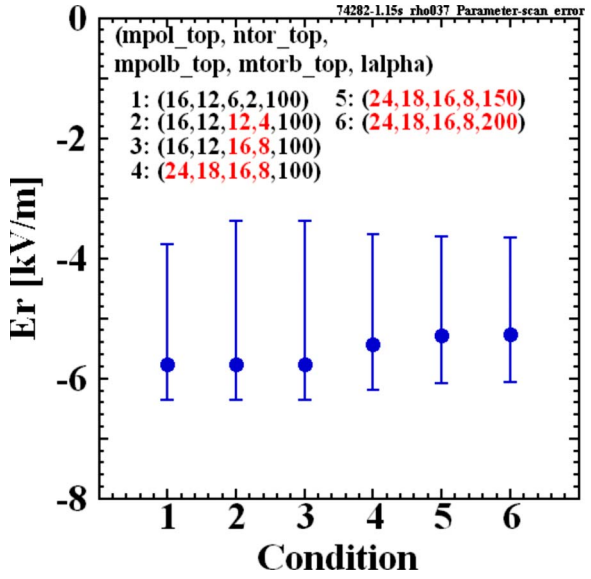

FIG. 10. (Color online) Ambipolar E_r evaluated at $\rho \sim 0.37$ for a higher-T_i case shown in Fig. 1(a) while varying the parameters used for the DKES calculations. The parameters are listed in the figure according to the condition number.

Further investigation will be extensively performed so that DKES can be properly and practically applied for NC transport analyses of high-T_i plasmas in LHD.

[1] A. Iiyoshi, A. Komori, A. Ejiri, M. Emoto, H. Funaba, M. Goto, K. Ida, H. Idei, S. Inagaki, S. Kado, O. Kaneko, K. Kawahata, T. Kobuchi, S. Kubo, R. Kumazawa, S. Masuzaki, T. Minami, J. Miyazawa, T. Morisaki, S. Morita, S. Murakami, S. Muto, T. Mutoh, Y. Nagayama, Y. Nakamura, H. Nakanishi, K. Narihara, K. Nishimura, N. Noda, S. Ohdachi, N. Ohyabu, Y. Oka, M. Osakabe, T. Ozaki, B. J. Peterson, A. Sagara, S. Sakakibara, R. Sakamoto, H. Sasao, M. Sasao, K. Sato, M. Sato, T. Seki, T. Shimozuma, M. Shoji, H. Suzuki, Y. Takeiri, K. Tanaka, K. Toi, T. Tokuzawa, K. Tsumori, K. Tsuzuki, K. Y. Watanabe, T. Watari, H. Yamada, I. Yamada, S. Yamaguchi, M. Yokoyama, R. Akiyama, H. Chikaraishi, K. Haba, S. Hamaguchi, M. Iima, S. Imagawa, N. Inoue, K. Iwamoto, S. Kitagawa, J. Kodaira, Y. Kubota, R. Maekawa, T. Mito, T. Nagasaka, A. Nishimura, C. Takahashi, K. Takahata, Y. Takita, H. Tamura, T. Tsuzuki, S. Yamada, K. Yamauchi, N. Yanagi, H. Yonezu, Y. Hamada, K. Matsuoka, K. Murai, K. Ohkubo, I. Ohtake, M. Okamoto, S. Satoh, T. Satow, S. Sudo, S. Tanahashi, K. Yamazaki, M. Fujiwara, and O. Motojima, Nucl. Fusion **39**, 1245 (1999).

[2] O. Motojima, H. Yamada, A. Komori, N. Ohyabu, T. Mutoh, O. Kaneko, K. Kawahata, T. Mito, K. Ida, S. Imagawa, Y. Nagayama, T. Shimozuma, K. Y. Watanabe, S. Masuzaki, J. Miyazawa, T. Morisaki, S. Morita, S. Ohdachi, N. Ohno, K. Saito, S. Sakakibara, Y. Takeiri, N. Tamura, K. Toi, M. Tokitani, M. Yokoyama, M. Yoshinuma, K. Ikeda, A. Isayama, K. Ishii, S. Kubo, S. Murakami, K. Nagasaki, T. Seki, K. Takahata, H. Takenaga, and the LHD Experimental Group, Nucl. Fusion **47**, S668 (2007).

[3] C. C. Petty, M. R. Wade, J. E. Kinsey, R. J. Groebner, T. C. Luce, and G. M. Staebler, Phys. Rev. Lett. **83**, 3661 (1999).

[4] S. Toda, K. Itoh, A. Fujisawa, S.-I. Itoh, M. Yagi, A. Fukuyama, P. H. Diamond, and K. Ida, Nucl. Fusion **47**, 914 (2007).

[5] M. Yokoyama, K. Ida, H. Sanuki, K. Itoh, K. Narihara, K. Tanaka, K. Kawahata, N. Ohyabu, and LHD Experimental Group, Nucl. Fusion **42**, 143 (2002).

[6] K. Ida, H. Funaba, S. Kado, K. Narihara, K. Tanaka, Y. Takeiri, Y. Nakamura, N. Ohyabu, K. Yamazaki, M. Yokoyama, S. Murakami, N. Ashikawa, P. C. de Vries, M. Emoto, M. Goto, H. Idei, K. Ikeda, S. Inagaki, N. Inoue, M. Isobe, K. Itoh, O. Kaneko, K. Kawahata, K. Khlopenkov, A. Komori, S. Kubo, R. Kumazawa, Y. Liang, S. Masuzaki, T. Minami, J. Miyazawa, T. Morisaki, S. Morita, T. Mutoh, S. Muto, Y. Nagayama, H. Nakanishi, K. Nishimura, N. Noda, T. Notake, T. Kobuchi, S. Ohdachi, K. Ohkubo, Y. Oka, M. Osakabe, T. Ozaki, R. O. Pavlichenko, B. J. Peterson,

A. Sagara, K. Saito, S. Sakakibara, R. Sakamoto, H. Sanuki, H. Sasao, M. Sasao, K. Sato, M. Sato, T. Seki, T. Shimzuma, M. Shoji, H. Suzuki, S. Sudo, N. Tamura, K. Toi, T. Tokuzawa, Y. Torii, K. Tsumori, T. Yamamoto, H. Yamada, I. Yamada, S. Yamaguchi, S. Yamamoto, Y. Yoshimura, K. Y. Watanabe, T. Watari, Y. Hamada, O. Motojima, and M. Fujiwara, Phys. Rev. Lett. **86**, 5297 (2001).

[7] T. Shimozuma, S. Kubo, H. Idei, Y. Yoshimura, T. Notake, K. Ida, N. Ohyabu, I. Yamada, K. Narihara, S. Inagaki, Y. Nagayama, Y. Takeiri, H. Funaba, S. Muto, K. Tanaka, M. Yokoyama, S. Murakami, M. Osakabe, R. Kumazawa, N. Ashikawa, M. Emoto, M. Goto, K. Ikeda, M. Isobe, T. Kobichi, Y. Liang, S. Masuzaki, T. Minami, J. Miyazawa, S. Morita, T. Morisaki, T. Mutoh, H. Nakanishi, K. Nishimura, N. Noda, S. Ohdachi, Y. Oka, T. Ozaki, B. J. Peterson, Y. Narushima, A. Sagara, K. Saito, S. Sakakibara, R. Sakamoto, M. Sasao, M. Sato, K. Satoh, T. Seki, S. Shoji, H. Suzuki, N. Tamura, K. Tokuzawa, Y. Torii, K. Toi, K. Tsumori, K. Y. Watanabe, T. Watari, S. Yamamoto, T. Yamamoto, M. Yoshinuma, K. Yamazaki, S. Sudo, K. Ohkubo, K. Itoh, A. Komori, H. Yamada, O. Kaneko, Y. Nakamura, K. Kawahata, K. Matsuoka, O. Motojima, and the LHD Experimental Group, Plasma Phys. Controlled Fusion **45**, 1183 (2003).

[8] Y. Takeiri, S. Kubo, T. Shimozuma, M. Yokoyama, M. Osakabe, K. Ikeda, K. Tsumori, Y. Oka, K. Nagaoka, Y. Yoshimura, K. Ida, H. Funaba, S. Murakami, K. Tanaka, B. J. Peterson, I. Yamada, N. Ohyabu, K. Ohkubo, O. Kaneko, A. Komori, and LHD experimental group, Fusion Sci. Technol. **46**, 106 (2004).

[9] M. Yokoyama, H. Maaßberg, C. D. Beidler, V. Tribaldos, K. Ida, T. Estrada, F. Castejon, A. Fujisawa, T. Minami, T. Shimozuma, Y. Takeiri, A. Dinklage, S. Murakami, and H. Yamada, Nucl. Fusion **47**, 1213 (2007).

[10] Y. Takeiri, S. Morita, K. Ikeda, K. Ida, S. Kubo, M. Yokoyama, K. Tsumori, Y. Oka, M. Osakabe, K. Nagaoka, T. Shimozuma, M. Yoshinuma, K. Narihara, H. Funaba, M. Goto, S. Inagaki, K. Tanaka, O. Kaneko, A. Komori, O. Motojima, and the LHD Experimental Group, Nucl. Fusion **47**, 1078 (2007).

[11] M. Yoshinuma, Stellarator News **111**, 6 (2007).

[12] O. Kaneko, Y. Takeiri, K. Tsumori, Y. Oka, M. Osakabe, K. Ikeda, K. Nagaoka, T. Kawamoto, E. Asano, and M. Sato, Nucl. Fusion **43**, 692 (2003).

[13] K. Saito, R. Kumazawa, T. Mutoh, T. Seki, T. Watari, Y. Torii, D. A. Hartmann, Y. Zhao, A. Fukuyama, F. Shimpo, G. Nomura, M. Yokota, M. Sasao, M. Isobe, M. Osakabe, T. Ozaki, K. Narihara, Y. Nagayama, S. Inagaki, K. Itoh, S. Morita, A. V. Krasilnikov, K. Ohkubo, M. Sato, S. Kubo, T. Shimozuma, H. Idei, Y. Yoshimura, O. Kaneko, Y. Takeiri, Y. Oka, K. Tsumori, K. Ikeda, A. Komori, H. Yamada, H. Funaba, K. Y. Watanabe, S. Sakakibara, M. Shoji, R. Sakamoto, J. Miyazawa, K. Tanaka, B. J. Peterson, N. Ashikawa, S. Murakami, T. Minami, S. Ohdachi, S. Yamamoto, S. Kado, H. Sasao, H. Suzuki, K. Kawahata, P. de Vries, M. Emoto, H. Nakanishi, T. Kobuchi, N. Inoue, N. Ohyabu, Y. Nakamura, S. Masuzaki, S. Muto, K. Sato, T. Morisaki, M. Yokoyama, T. Watanabe, M. Goto, I. Yamada, K. Ida, T. Tokuzawa, N. Noda, S. Yamaguchi, K. Akaishi, A. Sagara, K. Toi, K. Nishimura, K. Yamazaki, S. Sudo, Y. Hamada, O. Motojima, and M. Fujiwara, Nucl. Fusion **41**, 1021 (2001).

[14] Y. Takeiri, S. Morita, K. Tsumori, K. Ikeda, Y. Oka, M. Osakabe, K. Nagaoka, M. Goto, J. Miyazawa, S. Masuzaki, N. Ashikawa, M. Yokoyama, S. Murakami, K. Narihara, I. Yamada, S. Kubo, T. Shimozuma, S. Inagaki, K. Tanaka, B. J. Peterson, K. Ida, O. Kaneko, A. Komori, and LHD Experimental Group, Nucl. Fusion **45**, 565 (2005).

[15] Y. Takeiri, M. Yokoyama, K. Nagaoka, K. Ida, S. Kubo, T. Shimozuma, H. Funaba, M. Osakabe, K. Ikeda, K. Tsumori, Y. Oka, M. Yoshinuma, S. Morita, M. Goto, K. Narihara, I. Yamada, K. Tanaka, O. Kaneko, A. Komori, and LHD Experimental Group, "Improvement of ion confinement in core electron-root confinement (CERC) plasmas in Large Helical Device," Proceedings of the 16th International Stellarator/Heliotron Workshop, jointly with 17th International Toki Conference, Toki, 2007 [Plasma Fusion Res. (to be published)].

[16] K. Nagaoka, M. Yokoyama, Y. Takeiri, K. Ida, M. Yoshinuma, S. Morita, T. Mutoh, T. Seki, K. Ikeda, M. Osakabe, K. Tsumori, Y. Oka, O. Kaneko, and the LHD Experimental Group, "Ion heating experiments using perpendicular neutral beam injection in the Large Helical Device," Proceedings of the 16th International Stellarator/Heliotron Workshop, jointly with 17th International Toki Conference, Toki, 2007 [Plasma Fusion Res. (to be published)].

[17] S. Murakami, N. Nakajima, and M. Okamoto, Fusion Technol. **27**, 256 (1995).

[18] S. Murakami, H. Yamada, M. Sasao, M. Isobe, T. Ozaki, T. Saida, P. Goncharov, J. F. Lyon, M. Osakabe, T. Seki, Y. Takeiri, Y. Oka, K. Tsumori, K. Ikeda, T. Mutoh, R. Kumazawa, K. Saito, Y. Torii, T. Watari, A. Wakasa, K. Y. Watanabe, H. Funaba, M. Yokoyama, H. Maassberg, C. D. Beidler, A. Fukuyama, K. Itoh, K. Ohkubo, O. Kaneko, A. Komori, O. Motojima, and LHD Experimental Group, Fusion Sci. Technol. **46**, 241 (2004).

[19] C. D. Beidler and W. D. D'haeseleer, Plasma Phys. Controlled Fusion **37**, 463 (1995).

[20] K. Ida, M. Yoshinuma, M. Yokoyama, S. Inagaki, N. Tamura, B. J. Peterson, T. Morisaki, S. Masuzaki, A. Komori, Y. Nagayama, K. Tanaka, K. Narihara, K. Y. Watanabe, C. D. Beidler, and LHD Experimental Group, Nucl. Fusion **45**, 391 (2005).

[21] S. Matsuoka, M. Yokoyama, K. Nagaoka, Y. Takeiri, M. Yoshinuma, K. Ida, T. Seki, H. Funaba, S. Murakami, A. Fukuyama, N. Ohyabu, O. Kaneko, and the LHD Experimental Group, "Neoclassical transport properties in high-ion-temperature hydrogen plasmas in the Large Helical Device (LHD)," Proceedings of the 16th International Stellarator/Heliotron Workshop, jointly with 17th International Toki Conference, Toki, 2007 [Plasma Fusion Res. (to be published)].

[22] K. Nagashima, Y. Koide, and H. Shirai, Nucl. Fusion **34**, 449 (1994).

[23] K. Ida, Y. Miura, T. Matsuda, K. Itoh, S. Hidekuma, S.-I. Itoh, and JFT-2M Group, Phys. Rev. Lett. **74**, 1990 (1995).

[24] J. E. Rice, M. Greenwald, I. H. Hutchinson, E. S. Marmar, Y. Takase, S. M. Wolfe, and F. Bombarda, Nucl. Fusion **38**, 75 (1998).

[25] M. Yoshida, Y. Koide, H. Takenaga, H. Urano, N. Oyama, K. Kamiya, Y. Sakamoto, Y. Kamada, and the JT-60 Team, Plasma Phys. Controlled Fusion **48**, 1673 (2006).

[26] Ö. D. Gürcan, P. H. Diamond, T. S. Hahm, and R. Singh, Phys. Plasmas **14**, 042306 (2007).

[27] M. Yoshinuma, K. Ida, M. Yokoyama, K. Nagaoka, M. Osakabe, and the LHD Experimental Group, "Observation of toroidal flow on LHD," Proceedings of the 16th International Stellarator/Heliotron Workshop, jointly with 17th International Toki Conference, Toki, 2007 [Plasma Fusion Res. (to be published)].

[28] H. Wobig, H. Maaßberg, H. Renner, W VII-A Team, ECRH Group, and NI group, Plasma Phys. Controlled Nucl. Fusion Res. **2**, 369 (1987).

[29] K. Itoh, H. Sanuki, and S.-I. Itoh, Nucl. Fusion **32**, 1047 (1992).

[30] T. Mutoh, R. Kumazawa, T. Seki, K. Saito, H. Kasahara, Y. Nakamura, S. Masuzaki, S. Kubo, Y. Takeiri, T. Shimozuma, Y. Yoshimura, H. Igami, T. Watanabe, H. Ogawa, J. Miyazawa, M. Shoji, N. Ashikawa, K. Nishimura, M. Osakabe, K. Tsumori, K. Ikeda, K. Nagaoka, Y. Oka, H. Chikaraishi, H. Funaba, S. Morita, M. Goto, S. Inagaki, K. Narihara, T. Tokuzawa, R. Sakamoto, T. Morisaki, B. J. Peterson, K. Tanaka, H. Nakanishi, M. Nishiura, T. Ozaki, F. Shimpo, G. Nomura, C. Takahashi, M. Yokota, Y. P. Zhao, J. G. Kwak, S. Murakami, H. Okada, H. Yamada, K. Kawahata, N. Ohyabu, O. Kaneko, K. Ida, Y. Nagayama, K. Y. Watanabe, N. Noda, A. Komori, S. Sudo, and O. Motojima, Nucl. Fusion **47**, 1250 (2007).

[31] M. Yokoyama, H. Maaßberg, C. D. Beidler, V. Tribaldos, K. Ida, T. Estrada, F. Castejon, A. Fujisawa, T. Minami, T. Shimozuma, Y. Takeiri, A. Dinklage, S. Murakami, and H. Yamada, Nucl. Fusion **47**, 1213 (2007).

[32] K. Ida, T. Shimozuma, H. Funaba, K. Narihara, S. Kubo, S. Murakami, A. Wakasa, M. Yokoyama, Y. Takeiri, K. Y. Watanabe, K. Tanaka, M. Yoshinuma, Y. Liang, N. Ohyabu, and the LHD Experimental Group, Phys. Rev. Lett. **91**, 085003 (2003).

[33] S. P. Hirshman, K. C. Shaing, W. I. van Rij, C. O. Beasley, Jr., and E. C. Crume, Jr., Phys. Fluids **29**, 2951 (1986).

[34] H. Sugama and S. Nishimura, Phys. Plasmas **9**, 4637 (2002).

[35] S. Murakami, A. Wakasa, H. Maaßberg, C. D. Beidler, H. Yamada, K. Y. Watanabe, and LHD Experimental Group, Nucl. Fusion **42**, L19 (2002).

[36] N. Ohyabu, T. Morisaki, S. Masuzaki, R. Sakamoto, M. Kobayashi, J. Miyazawa, M. Shoji, A. Komori, and O. Motojima, Phys. Rev. Lett. **97**, 055002 (2006).